Plasma Science and Technology

PAPER

UV and soft x-ray emission from gaseous and solid targets employing SiC detectors

Plasma Sci. Technol. **23** (2021) 055508 (8pp) https://doi.org/10.1088/2058-6272/abf423

UV and soft x-ray emission from gaseous and solid targets employing SiC detectors

Alfio TORRISI[1], **Przemysław WACHULAK**[2] **and Lorenzo TORRISI**[3]

[1] CEDAD - Dept. of Mathematics and Physics 'E. De Giorgi', University of Salento, Lecce 73100, Italy
[2] Institute of Optoelectronics, Military University of Technology, Warsaw 00-908, Poland
[3] Dept. of Mathematical and Computer Sciences, Physical Sciences and Earth Sciences (MIFT)—University of Messina, Messina 98166, Italy

E-mail: alfio.torrisi@unisalento.it

Received 1 December 2020, revised 30 March 2021
Accepted for publication 31 March 2021
Published 6 May 2021

Abstract

A ns Nd:YAG pulsed laser has been employed to produce plasma from the interaction with a dense target, generating continuum and UV and soft x-ray emission depending on the laser parameters and target properties. The laser hits solid and gaseous targets producing plasma in high vacuum, which was investigated by employing a silicon carbide detector. The two different interaction mechanisms were studied, as well as their dependence on the atomic number. The photon emission from laser-generated plasma produced by solid targets, such as boron nitride (BN) and other elements (Al, Cu, Sn and Ta) and compounds such as polyethylene, has been compared with that coming from plasma produced by irradiating different gas-puff targets based on N_2 and other gases (Ar, Xe, Kr, SF_6). The experimental results demonstrated that the yields are comparable and, in both cases, increase proportionally to the target atomic number. The obtained results, focusing the attention on the advantages and drawbacks of the employed targets, are presented and discussed.

Keywords: laser–matter interaction, plasma diagnostics, SiC detectors

(Some figures may appear in colour only in the online journal)

1. Introduction

Although the main way to produce x-rays is based on the use of an x-ray tube in which energetic electrons hit a solid anode producing bremsstrahlung and characteristic x-ray emission, in the past, different sources employing various techniques have been developed. One of the most efficient methods consists of the employment of high-intensity pulsed lasers interacting with the matter. An important parameter to describe the laser–matter interaction producing plasma is represented by the electron plasma frequency, ω_c, defined as:

$$\omega_c = \sqrt{\frac{n_e e^2}{m\,\varepsilon_0}} \tag{1}$$

where n_e is the electron density, e is the electron charge, m is the electron mass and ε_0 is the vacuum permittivity. If $\omega > \omega_c$, the laser light with ω frequency penetrates in the plasma, meanwhile the laser is reflected. The use of a pulsed laser hitting a solid target or a double-stream gas-puff, synchronized with the laser shot, allows one to generate ultraviolet (UV) and x-ray emission. When a high-intensity laser (10^{10}–10^{12} W cm^{-2}) interacts with a solid surface, it produces ablation, gas ionization and plasma. If the non-equilibrium plasma has a high electron density, electrons are accelerated, and x-rays are generated [1]. In this case, UV and soft x-ray (SXR) emission are mainly produced by the electron bremsstrahlung with the high-density matter [1, 2]. Meanwhile, if the laser hits a gas target, which generally has low density (less than 10^{18} cm^{-3}), the laser propagates inside the plasma (undercritical plasma). The laser propagation produces electron oscillations, plasma waves, ionizations by the electron–atom interactions and excitations [3], and UV and x-ray plasma emission mainly produced by atom deexcitation processes. The photon emission generated by the solid and gas targets involves a different atomic density and different modalities of x-ray emission. Indeed, in the first instant of the ablation, for a solid target the plasma density generally has an electron density higher than 10^{18} cm^{-3}

(overcritical) and mainly continuum bremsstrahlung emission takes place, while for a gas target, which generally has a density in a range of 10^{14}–10^{18} cm^{-3}, soft x-rays mainly come out from deexcitation processes that have characteristic energies [4]. Although the x-ray intensity is lower, the employment of a gaseous target gives several advantages to the photon emission. In particular, it does not generate atoms and debris at emission angles higher than about 45° with respect to the incident laser direction. This is because the high pressure of the gas-puff is directional and the atoms, ions and clusters are mainly pushed in a forward direction and not laterally, according to the extensive literature on the subject [5].

Moreover, it can be used with repetitive laser shots to obtain repetitive photon emission, without the need to change the target, as would happen for ablation of solid targets [6]. Additionally, the produced SXR at large angles (90°) with respect to the incident laser beam drastically reduces the plasma ion emission in the direction of SXRs. Specifically, using a double-stream gas-puff target source it is possible to increase the plasma density along the emission direction, giving the result of a plasma density up to $\sim 10^{18}$ cm^{-3} and higher SXR emission intensities [7]. The SXR emission produced from a laser–gas-puff interaction is comparable in flux with that coming from a traditional x-ray tube allowing one to obtain about 10^{13} photons/pulse [8].

The photon emission from the investigated plasma was monitored using a fast 4H-SiC (silicon carbide) detector, with a higher energy gap compared to that of classical Si detectors, of 3.3 eV, which allows one to observe the UV and SXR plasma emitted without a background signal due to the visible light component [9].

In this work, the photon emission from laser-generated plasma produced by solid targets, such as boron nitride (BN) and other elements (polyethylene (PE), Al, Cu, Sn and Ta), will be compared with that coming from plasma produced by irradiating different gas-puff targets based on N_2 and other gases (i.e. Ar, Xe, Kr, SF_6). The aim of this work is to show the advantages of using a gas-puff target with respect to a solid one for the generation of UV and SXR emission and its photon emission monitoring using 4H-SiC detectors. The experimental results will be presented here and discussed, showing the advantages and disadvantages of the two techniques.

2. Experimental setup

An Nd:YAG pulsed laser ($\lambda = 1064$ nm, pulse energy of 0.69 J, pulse duration of 3 ns, frequency 10 Hz, spot of 0.5–1 mm^2 and maximum intensity of about 4.6×10^{10} W cm^{-2}) was employed to irradiate solid and gas-puff targets. The experimental setup is depicted in figure 1.

The laser pulse was focused in the vacuum chamber, where the samples are placed. The employment of a double-stream gas-puff target source, described in detail in [10], allows one to increase the gas density along the emission direction. Such a source is formed by two circularly concentric nozzles. The inner nozzle is circular, 0.4 mm in diameter and injects a small amount of working gas (N_2) into the vacuum. The concentric outer ring nozzle, 0.7–1.5 mm in diameter, injects a low-Z gas (helium), to reduce the working gas density gradient along the normal to the nozzle axis. Thus, one of the main advantages of employing this particular compact source is the possibility to obtain thousands of shots per day without debris production, avoiding laser absorption from clusters [11], as happens in the case of solid targets, and allowing one to obtain a plasma density of about 10^{18} atoms cm^{-3} [7]. Appropriate time synchronization of the valves between the gas-puff target formation and the arrival of the laser beam is required, for efficient SXR/EUV (SXR/extreme ultraviolet) radiation generation. A valve controller was synchronized with a synchronization output signal of the pumping laser. As the system works at 10 Hz repetition rate, the duration of one cycle was 100 ms. In our experiments, the outer gas pressure (helium) was set at 6 bar, while the working gas pressure spanned in a range from 2 to 10 bar, to obtain the highest possible gas flux.

The gas pressures were measured before the injection valve and not in vacuum. Opportune filters, placed between the target and the detector, allow one to select different plasma emissions in the SXR/EUV range [6]. The employed filters were made of Al, Ti, CaF_2 and Zr with thicknesses of 750 nm, 200 nm, 5 mm and 250 nm, respectively. They select the radiation from different wavelength ranges: Al operates within 16 and 60 nm; Ti filters in the range of 0.1–6 nm; CaF_2 filters in the range of 180–300 nm; and Zr operates in the range of 8–18 nm.

In a solid target, the interaction between the laser and the BN target has particularly been taken into account to compare the obtained results with those due to the laser–gas (N_2) irradiation. The employed solid target is a semi-crystalline BN hexagonal phase h-BN ceramic with 99.5% purity, a density of 2.1 g cm^{-3}, used as a sheet with 2 mm thickness and 2 cm^2 surface. The laser–target interaction produces plasma emitting photons, which reach a SiC Schottky diode [12, 13], realized by the junction between the 4H-SiC semiconductor and the Ni_2Si conductive surface thin film, 20 nm thick (see the geometrical scheme in figure 2(a) and optical microscope photograph of six detectors in figure 2(b)). The active region of the detector has 0.1 mm^2 surface and 25 μm depth when inversely polarized with 10 V. Its reverse current at room temperature is in the order of 1 pA, for the reverse bias of 10 V (figure 2(c)). Its detection efficiency for photons ranges between 3.3 eV (SiC gap energy) and about 20 keV. It also detects electrons and ions transmitted by the surface metallic thin film. Protons, for example, according to the detection efficiency plot reported in figure 2(d), are detected between about 3 keV and 10 MeV kinetic energy.

The SiC detector, employed in a time of flight (TOF) configuration, was connected to a fast storage oscilloscope and placed along the normal direction to the solid target surface (where the emission is maximum) at 44 cm target-detector distance. For the gas-puff target, SiC was placed at a distance of 17 cm from the nozzle and at about 90° angle with respect to the incident laser beam direction.

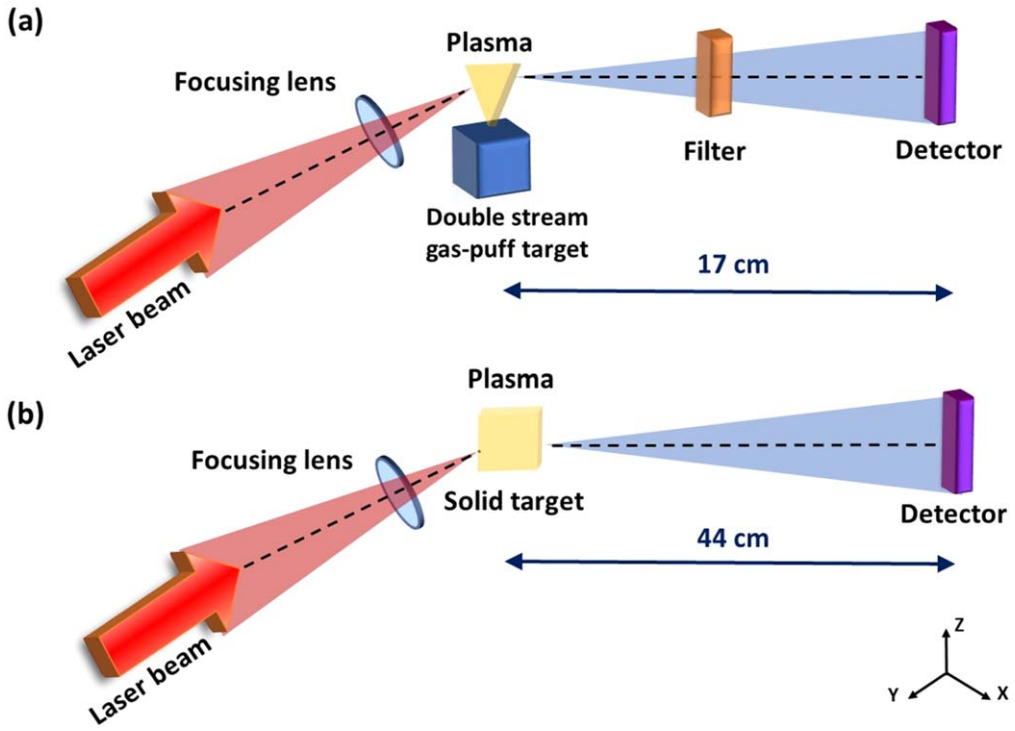

Figure 1. The experimental setup of the laser-plasma source hitting (a) a double-stream gas-puff target and (b) a solid target.

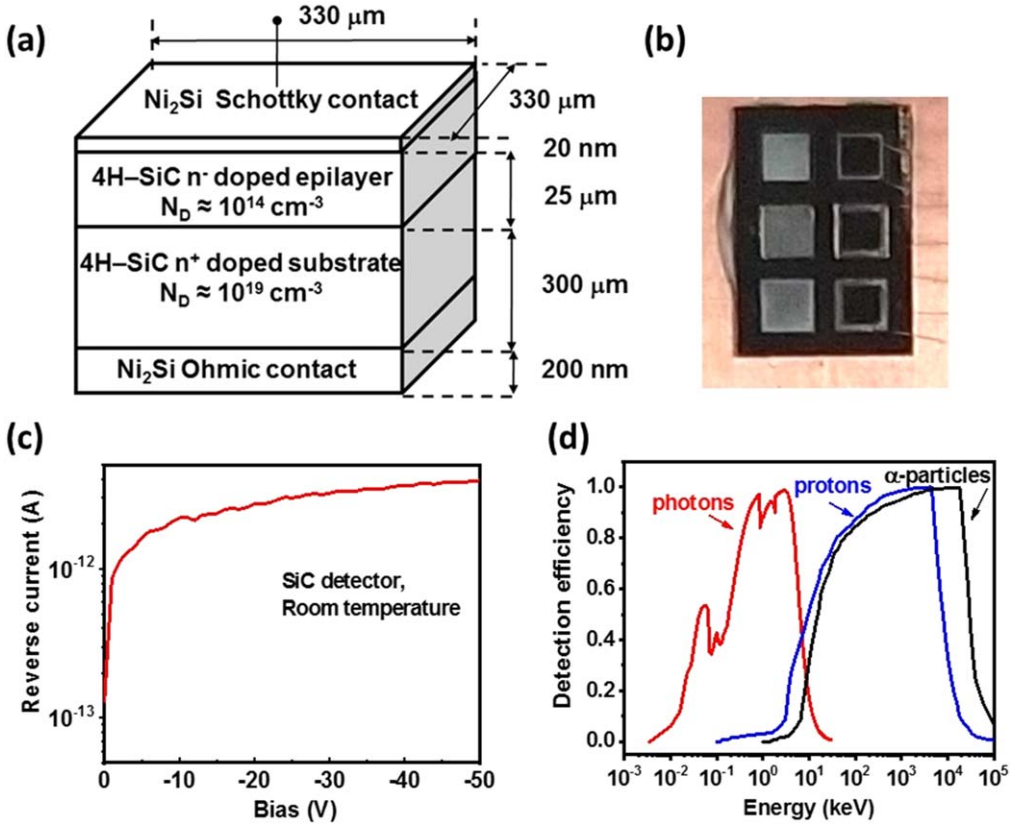

Figure 2. (a) A scheme and (b) photograph of six SiC detectors. (c) The reverse current (A) versus the bias (V), and (d) the detection efficiency of the detector versus energy (keV) for photons, protons and α-particles.

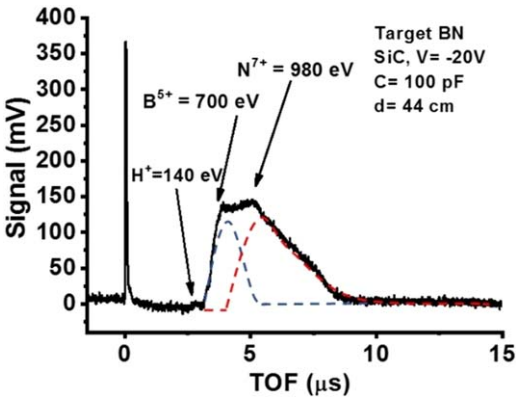

Figure 3. TOF spectra of plasma emission from a solid BN target.

SiC detects the faster photopeak due to the emission of UV and SXR from the produced plasma (which fixes the zero TOF scale) and the slower ions coming from the plasma and reaching the detector with different TOF values, depending on their velocity. The ionization potentials of the elements vs their charge states were obtained using the NIST database [14]. The evaluations of the SXR transmissions in the used filters vs photon energy and thickness were performed using the CXRO database [15].

3. Results and discussion

The plasma emission from the solid BN target irradiated in high vacuum (10^{-6} mbar) by a single laser pulse at 0.69 J energy, focused on a 0.5 mm^2 surface, was investigated using a SiC in TOF approach, as shown in figure 3. The spectrum was acquired using a detector bias of −20 V and a capacitive coupling to the storage oscilloscope input of 100 pF. It shows a prompt photopeak, due to the detection of UV and SXR, taken as a trigger signal for the TOF scale, and an ion peak represented by the convolution of protons, boron and nitrogen detected ions.

On the basis of the flight length (44 cm) and of the measured TOF value, it is possible to determine the maximum proton, boron and nitrogen ion velocities and their maximum kinetic energies. The maximum energy, calculable from the large ion peak shape in the discontinuity points, was 140 eV, 700 eV and 980 eV for protons, boron and nitrogen ions, respectively. The detected protons are derived by the hydrogen target surface contamination. The maximum boron charge state of 5+ can be obtained by dividing the maximum boron energy by that of protons. Similarly, the maximum nitrogen charge state of 7+ can be obtained by dividing the maximum nitrogen energy by that of protons. The ion acceleration, in fact, is due to the electric field that develops between the target-emitted electron cloud and the positively charged target. This electric field, which is proportional to the plasma electron density and temperature [16], drives both the protons and the ion acceleration, which increase proportionally to their charge state. The ion peak is the convolution of all charge states of produced ions, as reported in the Boltzmann

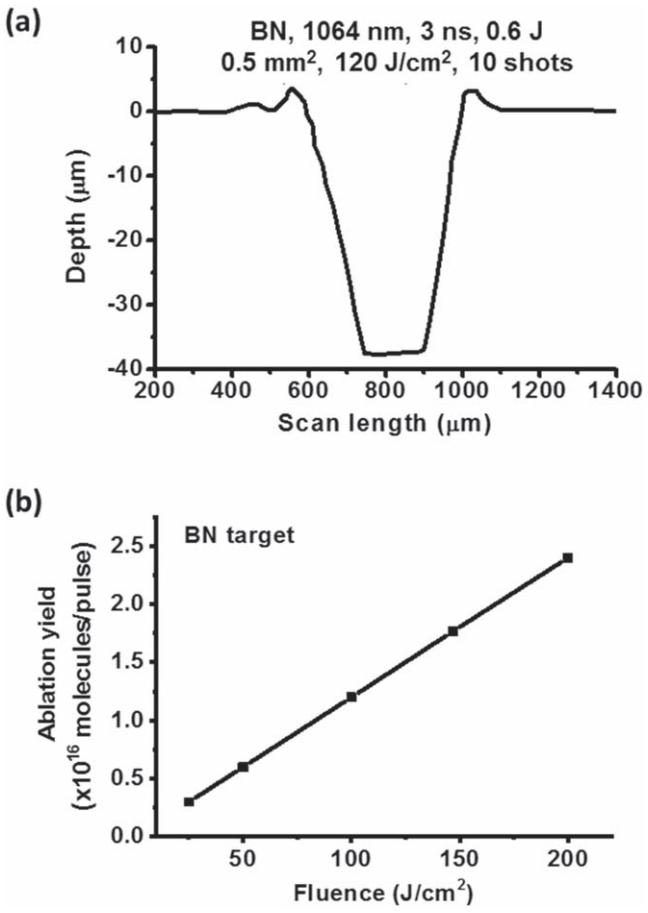

Figure 4. (a) A profile of the crater created on the BN target after ten laser shots at an energy of 100 J cm^{-2}, and (b) ablation yield (molecules per laser pulse) as a function of the laser fluence.

ion deconvolution of figure 3. The ion peak tail is due to the detection of slower ions at a single charge state. The ionization potentials of B^{5+} and N^{7+} are 340 eV and 667 eV, respectively, according to the NIST database [14]. Thus, plasma accelerates electrons at energies higher or comparable to 667 eV, being able to ionize nitrogen up to 7+. Assuming that the plasma electrons have a Boltzmann energy distribution with a maximum energy of cut-off at about 670 eV and that the mean electron energy E is about one sixth of this maximum value, i.e. about 112 eV, the equivalent plasma temperature of this non-equilibrium plasma is approximately given by:

$$kT = \frac{2}{3}E \sim 74\ \text{eV}. \tag{2}$$

The laser ablation of the solid BN target was monitored in terms of removed mass per laser pulse by measuring the removed mass produced by ten laser shots at 100 J cm^{-2} fluence. From this, a surface profile was acquired using the Tencor P10 instrument, obtaining the surface scanning profile reported in figure 4(a). The volume of the crater is 2.4×10^6 μm^3; thus, by considering the BN mass density of 2.1 g cm^{-3} (5×10^{22} molecules cm^{-3}), the corresponding removed mass is 5 μg and the ablation rate is 0.5 μg/pulse. The ablation yield, given in terms of emitted molecules per laser pulse,

corresponds to 1.2×10^{16} BN molecules/pulse. When the laser fluence is increased, the ablation yield increases linearly, as reported in the plot of figure 4(b).

The presented results are in good agreement with our previous investigations on laser-generated plasma from a BN target [17]. In the gas targets, the gas leak is regulated by a leak aperture time of 1 ms with different pressures ranging between 2 bar and 10 bar. At about 0.15 ms the 3 ns laser shot starts hitting the gas target with a spot size of 1 mm^2. Thus, it is possible to give the density of the gas by applying the adiabatic gas expansion velocity, v_k, in vacuum at room temperature [18]:

$$v_k = \sqrt{\frac{\gamma\, kT}{m}} \tag{3}$$

where γ is the adiabatic coefficient, k is the Boltzmann constant, T is the temperature and m is the atomic or molecular mass of the expanding gas. For N_2 molecules at room temperature ($\gamma = 1.4$, $T = 298$ K and $m = 28$ amu) $v_k = 3.5 \times 10^2$ m s^{-1} and the expansion length in 0.15 ms is $L = 5.3$ cm. The gas emitted in the vacuum chamber has an ellipsoidal shape in which L is the major axis, while the minor axes are approximately 1.4 cm each, according to the SXR backlighting images presented in a previous paper [19]. Thus, the ellipsoid gas volume is about 5.4 cm^3. Measurements of absolute N_2 gas pressure variation of $\Delta P = 1 \times 10^5$ Pa were obtained from a $V_0 = 10$ cm^3 container volume, which was opened with an electronic gate for 1 ms in high vacuum through the used nozzle device. This measure gives the number of injected molecules:

$$N = \frac{\Delta P \times V_0}{kT} = 2.4 \times 10^{20}\ \mathrm{N_2}\ \text{molecules}. \tag{4}$$

Thus, considering the 15% of such molecules injected in 0.15 ms, the gas density is:

$$\rho = \frac{N}{V} = \frac{3.6 \times 10^{19}}{5.4\ \mathrm{cm^3}} = 6.67 \times 10^{18}\ \text{molecules cm}^{-3}. \tag{5}$$

This calculation is in agreement with the literature, which reports that the density of this gas, emitted along the nozzle axis in a non-isotropic emission, is of the order of 10^{18} atoms cm^{-3} [20], i.e. it is about four orders of magnitude lower with respect to the BN solid target. Considering the gas-puff angular aperture emission ($\pm 15°$) and the laser spot distance from the nozzle (10 mm), the laser pulse hits an approximate volume of about 10 mm^3 (see the scheme of figure 5(a)). Thus, the single laser shot hits about 10^{16} atoms, a value comparable with the atomic ablation yield measured for the laser–solid matter interaction at 80 J cm^{-2} fluence (figure 4(b)).

In the SiC-TOF spectra generated by the laser irradiated gas targets, it is possible to observe only the photopeak, due to UV and SXR detection, without detection of ion peaks also at high TOF values. This result indicates that there is no ion emission from plasma at a 45°–90° angle from the laser incident direction. Figure 6 shows the SiC spectra of UV and SXR emitted by the nitrogen plasma for different gas pressures and detected as a function of the time from the laser shot.

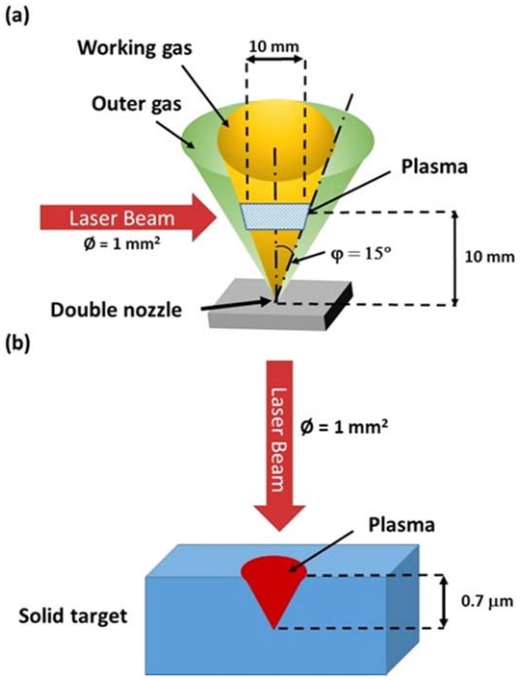

Figure 5. A scheme of laser–matter interaction with (a) a gas-puff target and (b) a solid target.

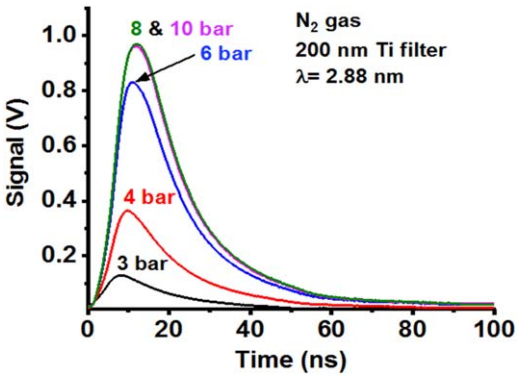

Figure 6. The N_2 gas-puff target as a function of the time, for different pressures, using a 200 nm Ti filter.

The spectra were acquired using a 200 nm Ti filter allowing us to obtain a quasi-monochromatic SXR emission from N_2, at 2.88 nm. A saturation signal is obtained for the N_2 pressure of 8–10 bar.

The detected photopeaks by laser irradiation of the solid and gas targets have three similar features, which will be considered as follows.

(i) The first factor concerns the different solid angle of detection because the SiC was placed at a distance of 17 cm from the centrum of the gas-puff target and at 44 cm from the solid target. In the two cases, the solid angle of detection is 3.5 μSr for the gas target and 0.52 μSr for the solid target. The photopeak intensities for irradiation of solid BN (at a pressure of 10^{-6} mbar) and of the N_2 gas (at a pressure of 8–10 bar) are 375 mV (figure 3) and 0.95 V (figure 6), respectively. In the employed experimental conditions, our measurements

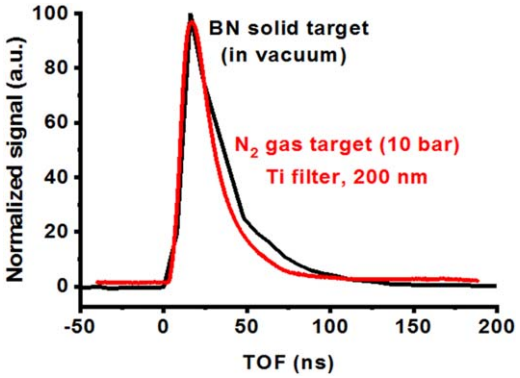

Figure 7. Comparison of the normalized photopeaks detected for the N_2 gas-puff target at a pressure of 10 bar with the solid BN target.

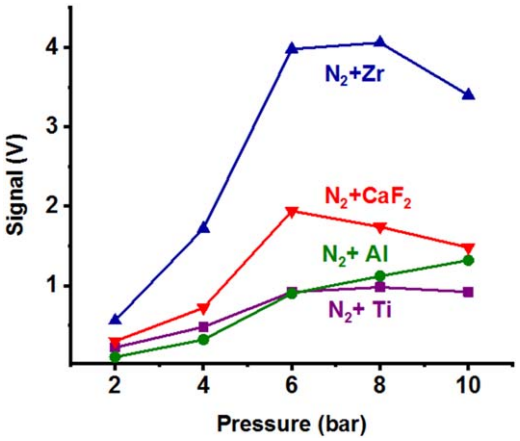

Figure 8. The photon emission signal vs the N_2 gas-puff target pressures for different absorber filters. Increasing the gas pressure, the proportionality is less linear, showing a saturation for high-pressure values.

have permitted us to evaluate a total photon emission per solid angle of detection of 721 mV/μSr and 271 mV/μSr for solid and gas targets, respectively.

(ii) The second factor takes into account the photopeak's correlation to the photon emission from very different density targets. Such values correspond to 5×10^{22} BN molecules cm^{-3} for the solid target and $\sim 10^{18}$ N_2 molecules cm^{-3} for the gas-puff target. However, the number of atoms per cm^2 hit by laser radiation is similar. In fact, considering that the penetration depth of the IR laser in BN is about 0.7 μm [21] (figure 5(b)) and about 10 mm in the gas-puff, the areal densities of the invested molecules are about 3.5×10^{18} molecules cm^{-2} and 10^{18} molecules cm^{-2} for the solid and gas targets, respectively. On the other hand, due to the small penetrating laser shot in BN, the number of ablated molecules for the solid phase is about 10^{16} per pulse at 80 J cm^{-2} laser fluence (figure 4(b)). This number is comparable with that of the hit molecules in the gas phase of about 10^{16} per pulse, being 1 mm^2 in laser spot size and 10 mm in penetration length.

(iii) The third factor is related to the two different mechanisms of photon emissions occurring in the two targets. Although the SiC photopeak shows a similar integral electric signal, it is generated by a continuum band emission due to electron bremsstrahlung as the main component emitted from the solid [1] and by a discrete and characteristic UV and SXR emission, due to atomic deexcitations, as the main component emitted from the gas [22, 23].

The comparison of the photopeaks, detected for the maximum N_2 gas-puff target (10 bar) and for the solid BN target, employing a 200 nm Ti filter, is reported in the normalized spectra of figure 7.

Although many differences in the two plasmas occur, the two integral photopeaks are similar. In fact, the pulse durations (in terms of full width half maximum, FWHM), are about 25 ns and 30 ns for the gas target and the BN target, respectively. The photopeak signal intensity is I_s =375 mV for the BN solid target and I_g=950 mV for the N_2 gas-puff target (at the pressure of 8–10 bar). The photon yield Y is measured in mV · ns. However, to compare the yields obtained by irradiating the solid and the gas targets, it was calculated with respect to the solid angle subtended by the detector.

Then, considering the product of the signal intensity I_s(mV) by the pulse duration (ns), evaluated by the FWHM and dividing by the subtended solid angle of the detector (steradiant, Sr), using s for solid and g for gas targets, we obtain, in the two cases:

$$Y_s = \frac{I_s \times \mathrm{FWHM}}{\Delta\Omega} = \frac{375(\mathrm{mV}) \times 30(\mathrm{ns})}{0.52(\mu\mathrm{Sr})} = 21.63 \frac{\mathrm{mV} \times \mathrm{s}}{\mathrm{Sr}} \quad (6)$$

$$Y_g = \frac{I_g \times \mathrm{FWHM}}{\Delta\Omega} = \frac{950(\mathrm{mV}) \times 25(\mathrm{ns})}{3.5(\mu\mathrm{Sr})} = 6.79 \frac{\mathrm{mV} \times \mathrm{s}}{\mathrm{Sr}}. \quad (7)$$

Thus, as expected for the higher target density, the UV and SXR yield for the plasma generated by the laser–solid impact gives a Y value approximately 3.2 times higher with respect to that generated by the laser–gas impact. However, the two photon yields remain comparable as orders of magnitude. This result also depends on the different laser depth penetration limited to about 1 μm and 10 mm, for the solid and gas-puff targets, respectively.

Preliminary measurements of the emitted photons indicate that the UV and x-ray emission obtained using the gas-puff targets seem to have a larger angular distribution with respect to the solid target [17, 24]. For the solid, in fact, the emission angle is limited by the aperture of the ablated crater geometry.

In the gas-puff target, the electrical signal of the UV and SXR detection grows with the gas pressure. Figure 8 reports the UV and SXR emission for an N_2 gas-puff target as a function of the gas pressure (2–10 bar) and of the type of absorber filter placed in front of the detector, according to previous measurements reported in the literature [5]. The data were acquired using the filters given in the experimental section (Al, Ti, CaF_2 and Zr with thicknesses of 750 nm, 200 nm, 5 mm and 250 nm, respectively). They select the

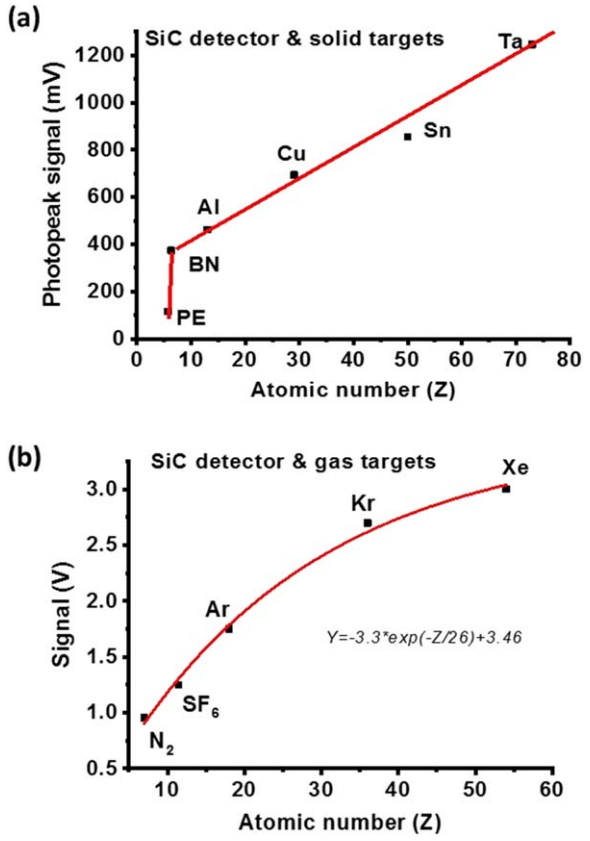

Figure 9. Photopeak signal dependence versus atomic number for (a) solid and (b) gas-puff targets.

radiation from different wavelength ranges, as discussed in the experimental section. The photon emission was detected at large angles, more than $\pm$ 45°. When the gas pressure is increased, the photon signal grows not linearly but exponentially, showing a saturation at high gas pressures.

The experiments of laser interaction with solid and gas targets were performed by also employing different solid targets and gases, to study the dependence of the UV and SXR yield on the atomic number Z of the irradiated targets. In both cases, it was found that the photopeak yield increases with the atomic number of the target.

Figure 9(a) presents the results obtained using different solid targets irradiated under the same experimental conditions with Z ranging between 6 (C) and 73 (Ta) and measuring the photopeak signal vs Z. For solid targets, the dependence is linear for metals but not for insulators, such as PE polymers. According to the bremsstrahlung emission theory, the x-ray production cross-section increases with Z^2/M^2, where Z is the atomic number of the target and M is the mass of the incident charge particles [25]. The obtained results do not confirm the Z^2 dependence of the photon signal; a linear growth with Z is observed for solid targets, while an exponential trend with a saturation is observed for gas targets. Figure 9(b) shows the peak signal dependence on the atomic number of the gas-puff target using a 10 bar pressure for different gases (N_2, SF_6, Ar, Kr and Xe), irradiated under the same experimental conditions. The signal increases with the atomic number with an exponential law tending to saturation at high atomic numbers. The obtained results reported in figure 9(b) show an exponential growth of the photon emission with Z and saturation for heavy atomic gases, indicating a significant divergence from the simple bremsstrahlung cross-section process. The photon emission, in fact, is due to the different mechanisms producing x-rays in the laser-generated plasma, so is the characteristic atomic fluorescence, the electron and ion bremsstrahlung, the secondary electron bremsstrahlung, and the blackbody radiation emission from the hot generated plasma plume [26].

4. Conclusions

A SiC detector was employed to investigate the photon emission from laser-generated plasma using a 3 ns laser at 690 mJ, irradiating solid targets (BN, PE, Al, Cu, Sn and Ta) and gas-puff targets (N_2, SF_6, Ar, Kr and Xe) in vacuum, to study and compare the different physical effects characterizing such laser–matter interactions. In the 2 mm thick BN, the plasma emission was investigated in terms of laser ablation yield, kinetic energies of the emitted ions, and photon emission of UV and SXR. The SXR emission could be due to fluorescence emission from nitrogen and boron and electron bremsstrahlung in the solid target. However, further spectroscopic measurements will be performed to acquire information about the photon energy distribution. This emission has a shape distribution similar to that of a blackbody [1] at 74 eV temperature, which, for the Wien law, has a maximum spectral emission of about $\lambda_{max} = 2.9 \times 10^{-3}$ mK/T_e(K) = 3.38 nm, corresponding to a photon energy $E = 366$ eV.

The detected UV and SXR from the gas targets are mainly due to the deexcitation of the atomic species, as neutral and as ionized, as reported in the literature [27]. The UV and SXR emission yields obtained from both experiments, performed under the same laser conditions, are similar. Indeed, the results show that a yield of 21.63 (mV×s)/Sr and 6.79 (mV×s)/Sr is obtained for solid targets (BN) in vacuum and for gas-puff (N_2) at 10 bar pressure, respectively. Thus, although the plasma density for gas targets is about four orders of magnitude lower with respect to that of the first instant of solids laser irradiating, the total emitted yield is comparable in the two cases. This is due to the major laser penetration in the low gas density (undercritical plasma) of the gas-puff target with respect to less penetration in the higher density of the solid target (overcritical plasma).

Both yields coming from solid and gas targets increase with the atomic number of the target showing a possible saturation trend at high atomic numbers for gas-puff targets. In the solid target, the x-ray emission is accomplished by atomic and molecular emission, and sometimes also by micro-cluster emissions and debris, while in the gas target, this corpuscular emission is negligible and absent at large angles with respect to the laser incidence direction. Thus, to build a clean UV or SXR source, such as for x-ray microscopy applications, it is possible to use both solid and gas-puff targets. The advantages of using gas targets will be mainly due to the low emission of micro-clusters and debris, while

the advantages of using solid targets is mainly due to the higher photon emission yield. However, although some emission spectra for solid and gas-puff targets were already acquired in different wavelength ranges [11, 28], a better comparison should be performed using adequate monochromatic spectrometers to analyze the photon emission in the two cases and to better distinguish the differences in wavelength ranges, intensity, photon energy and angular distributions of the spectral emissions.

ORCID iDs

Alfio TORRISI https://orcid.org/0000-0003-2404-5062

References

[1] Giulietti D and Gizzi L A 1998 *Riv. Nuovo Cim.* **21** 1
[2] Torrisi L, Torrisi A and Cutroneo M 2020 *Contrib. Plasma Phys.* **60** e202000012
[3] Eliezer S 2002 *The Interaction of High-Power Lasers with Plasmas* (Bristol: Institute of Physics Publishing)
[4] Hafez M A *et al* 2003 *Plasma Sources Sci. Technol* **12** 185
[5] Wachulak P W *et al* 2010 *Nucl. Instrum. Methods Phys. Res.* B **268** 1692
[6] Torrisi A *et al* 2019 *Phys. Rev. Accel. Beams* **22** 052901
[7] Wachulak P *et al* 2019 *APL Photonics* **4** 030807
[8] Pepper S V and Wheeler D R 2000 *Rev. Sci. Instrum.* **71** 1509
[9] Torrisi L *et al* 2009 *J. Appl. Phys.* **105** 123304
[10] Torrisi A *et al* 2020 *Appl. Sci.* **10** 8338
[11] Wachulak P W *et al* 2010 *Appl. Phys.* B **100** 461
[12] Bertuccio G and Casiraghi R 2003 *IEEE Trans. Nucl. Sci.* **50** 175
[13] Torrisi A *et al* 2017 *IEEE Trans. Electron Dev.* **64** 1120
[14] NIST Atomic Spectra Database Ionization Energies Form, https://physics.nist.gov/PhysRefData/ASD/ionEnergy.html
[15] CXRO Center for X-ray optics database, http://henke.lbl.gov/optical_constants/
[16] Torrisi L, Cutroneo M and Torrisi A 2020 *Contrib. Plasma Phys.* **60** e201900076
[17] Torrisi L and Torrisi A 2019 *Radiat. Eff. Defects Solids* **174** 76
[18] Torrisi L 2016 *Radiat. Eff. Defects Solids* **171** 34
[19] Fiedorowicz H *et al* 2000 *Appl. Phys.* B **70** 305
[20] Rakowski R *et al* 2010 *Appl. Phys.* B **101** 773
[21] Moscicki T 2016 *Int. J. Opt.* **2016** 5438721
[22] Bartnik A *et al* 2016 *Plasma Phys. Control. Fusion* **58** 014009
[23] Rakowski R *et al* 2011 *Appl. Phys.* B **102** 559
[24] Láska L *et al* 2002 *Rev. Sci. Instrum.* **73** 654
[25] Seltzer S M 1988 Cross sections for bremsstrahlung production and electron impact ionization *Monte Carlo Transport of Electrons and Photons* ed T M Jenkins *et al* (New York: Plenum)
[26] Yang X and Wei B 2016 *Sci. Rep.* **6** 37214
[27] Kanaev A V and Petitet J P 2004 *J. Appl. Phys.* **96** 4483
[28] Museur L *et al* 2007 *J. Lumin.* **127** 595